

# Supplementary Information for

## Towards High Quality Transferred Barium Titanate Ferroelectric Hybrid Integrated Modulator on SOI Platform

*Mengxue Tao<sup>1</sup>, Butong Zhang<sup>2</sup>, Tianxiang Zhao<sup>1</sup>, Xiaoxuan Wu<sup>1</sup>, Ming Liu<sup>2</sup>, Guohua Dong<sup>2,\*</sup>,  
and Junjia Wang<sup>1,\*</sup>*

<sup>1</sup>Address: National Research Center for Optical Sensors/communications Integrated  
Networks, School of Electronic Science and Engineering, Southeast University, 2 Sipailou,  
Nanjing, 210096, China  
E-mail: [junjia\\_wang@seu.edu.cn](mailto:junjia_wang@seu.edu.cn)

<sup>2</sup>Address: State Key Laboratory for Manufacturing Systems Engineering, Electronic Materials  
Research Laboratory, Key Laboratory of the Ministry of Education, Engineering  
Research Center of Spin Quantum Sensor Chips, Universities of Shaanxi Province,  
School of Electronic Science and Engineering, Xi'an Jiaotong University,  
Xi'an 710049, China

Email: [guohuadong@xjtu.edu.cn](mailto:guohuadong@xjtu.edu.cn)

## Supporting Note 1: SOI structure

On the silicon substrate, the silicon waveguide is buried in the oxide layer. The width of the buried silicon waveguide  $W_{Si}$  is 500 nm and the thickness  $t_{Si}$  is 220 nm. The thickness of the silicon oxide layer  $t_2$  is 2  $\mu\text{m}$ , as shown in Figure S1. We use a standard chemical mechanical planarization (CMP) technique to flat the top of the waveguide, leaving a thin layer of  $\text{SiO}_2$   $t_1 = 5$  nm on top.

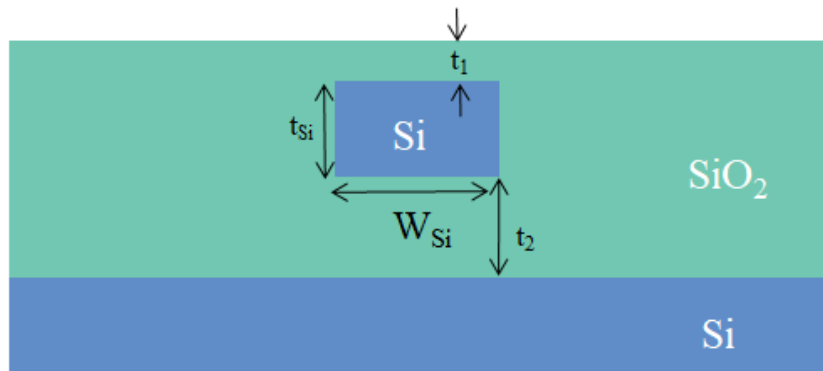


**Figure S1.** Schematic waveguide cross-section for SOI platform.

## Supporting Note 2: Optical images of BTO films

Fig. S2 shows a sample of BTO film transferred onto a gold-coated silicon wafer using the photoresist transfer method, the thickness of the sample is 150 nm with a size of about 2×2mm.

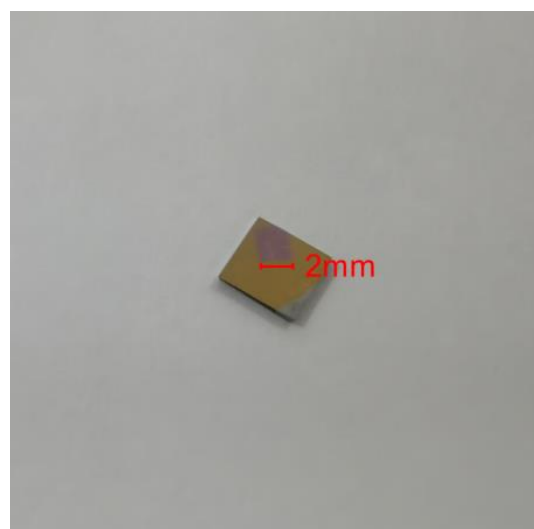


**Figure.S2.** Optical image of BTO film transferred onto a gold-coated silicon wafer.

### Supporting Note 3: AFM images of BTO films

In the experiment, we pay attention to control the surface roughness of the BTO samples. Via pulsed laser deposition method, high-quality BTO/SAO heterojunction was epitaxially grown on 3 mm \* 3 mm STO single crystal substrates. AFM image of the 150 nm BTO films surface is given in Fig. S2, the average roughness  $R_q$  value is  $\sim 1.32$  nm.

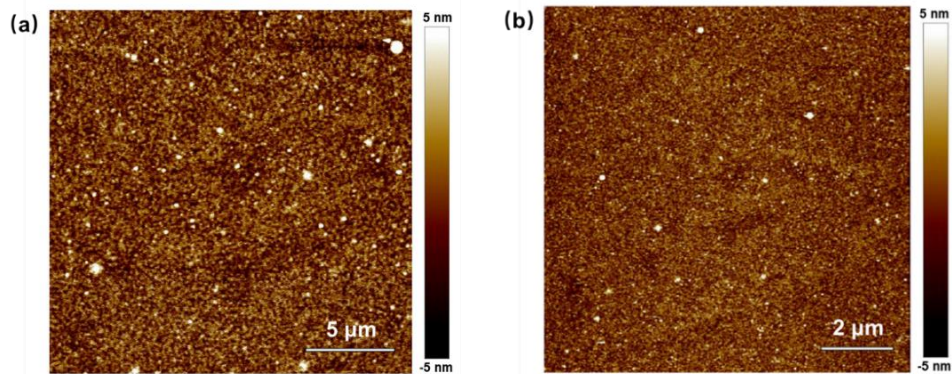


**Figure S3.** In-situ AFM images of BTO films (a) large area (b) smaller area.

### Supporting Note 4: Transfer process

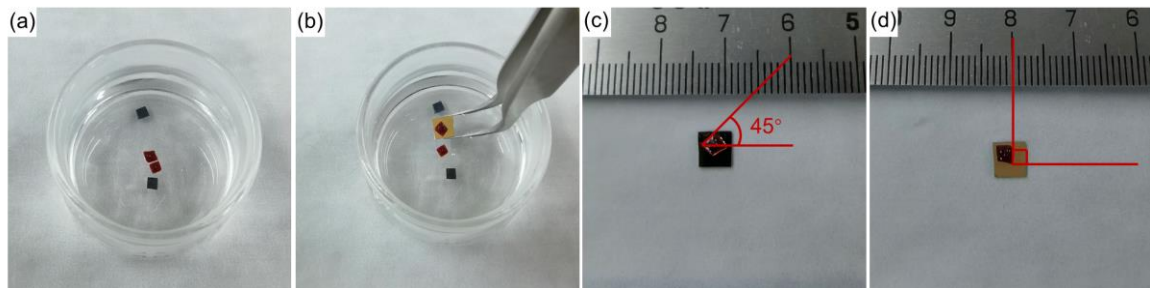


**Figure S4.** The transfer process using photoresist as a supporting layer. (a) Optical image of photoresist-BTO two-layer heterostructure floating on deionized water. (b) A demonstration of utilizing a target substrate to scoop up the sample. (c-d) Optical images of the sample transferred onto the target substrate, and the orientation of the sample to the edge of the square target substrate was adjusted to 45 degrees and 90 degrees respectively.

Fig. S4 demonstrate the transfer process using photoresist as a supporting layer. In the transfer process, we coated a layer of 60-80  $\mu\text{m}$  positive photoresist (AR-P 3510T, Allresist GmbH) on the surface of the BTO using a spin coater. Compared with the nanoscale BTO layer, the hard supporting photoresist layer was quite enough to keep the sample flat and intact. After the film

was transferred to the target substrate, its orientation relative to the substrate could be adjusted freely before the sample was completely dry.

### Supporting Note 5: XRD patterns before and after transfer

Fig. S5 illustrates the lattice orientation of the STO/SAO/BTO films before and after the transfer as tested by X-ray diffraction (XRD), where before and after the transfer are shown in blue and red, respectively. And from the local magnification on the right, we can clearly observe that the angle change corresponding to the peak of the BTO diffraction peaks before and after the transfer is 0.409 degrees.

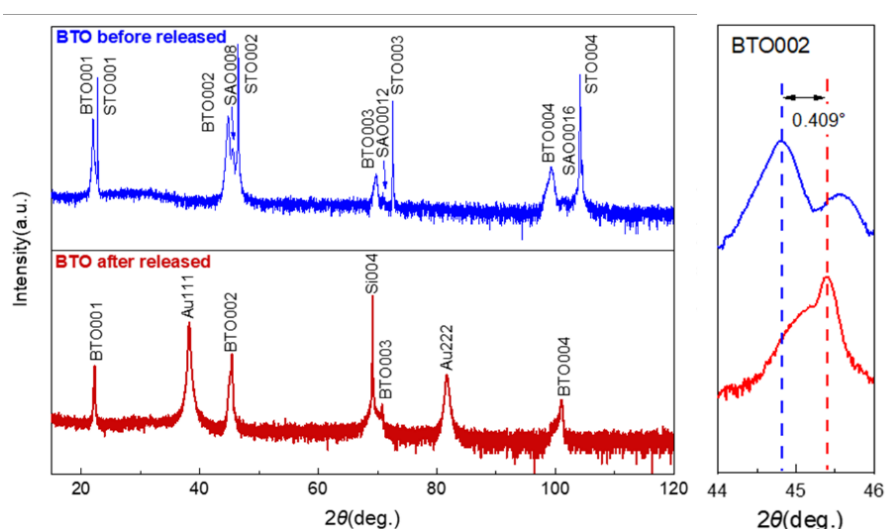
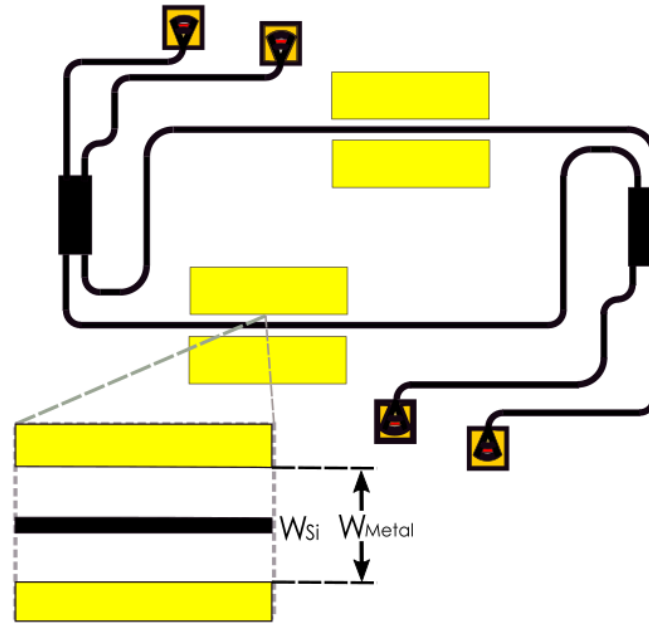


Figure S5. XRD patterns of STO/SAO/BTO films before and after transfer.

### Supporting Note 6: Design of the modulator structure

Our Mach-Zehnder interferometers (MZIs) structure consists of two  $2 \times 2$  multimode interferometers (MMI), two arms with different length and four grating couplers. A Mach-Zehnder interferometer has two waveguide arms of different lengths that receive essentially equal amounts of input signal. The different lengths of the arms produce a phase difference between them. The imbalanced arms result in an interference structure with a free spectral range of 2 nm. The contacts are placed at both sides of the silicon waveguide, as shown in Figure S6. The light is coupled in and out of the device by grating couplers. Once the applied voltage is

changed, cause the refractive index of the BTO layer on the waveguide to change, thus affecting the phase of the light at the output end. This phase change creates a shift of the resonance frequency which can be observed by scanning the laser at the same time.



**Figure S6.** Schematic of the Mach-Zehnder modulator, with a zoom in view of the contacts in the lower left corner. The black line represents the silicon waveguide, and the contacts located on both sides of the waveguide are shown in yellow. The width of the silicon waveguide  $W_{Si}$  is 0.5  $\mu\text{m}$  and the gap between the contacts  $W_{Metal}$  is 4  $\mu\text{m}$ .

### Supporting Note 7: Device testing

We test the EO response of MZMs with an active length of 286  $\mu\text{m}$  at different applied voltages. Figure S7 shows the experimental setups for EO measurement, containing a fibre laser, an optical polarizer, a DC power supply, a single-mode fibre, an amplifier, a detector and other devices. We can set the polarization state of the input light as TE mode through a fibre optic polarization controller. A DC power supply applies different voltages to the metal contacts via probes. The optical output of the modulator is amplified by a broadband erbium-doped fibre amplifier (EDFA) and filtered by a tunable filter. The signal is then collected by a PD and converted to electrical signal.

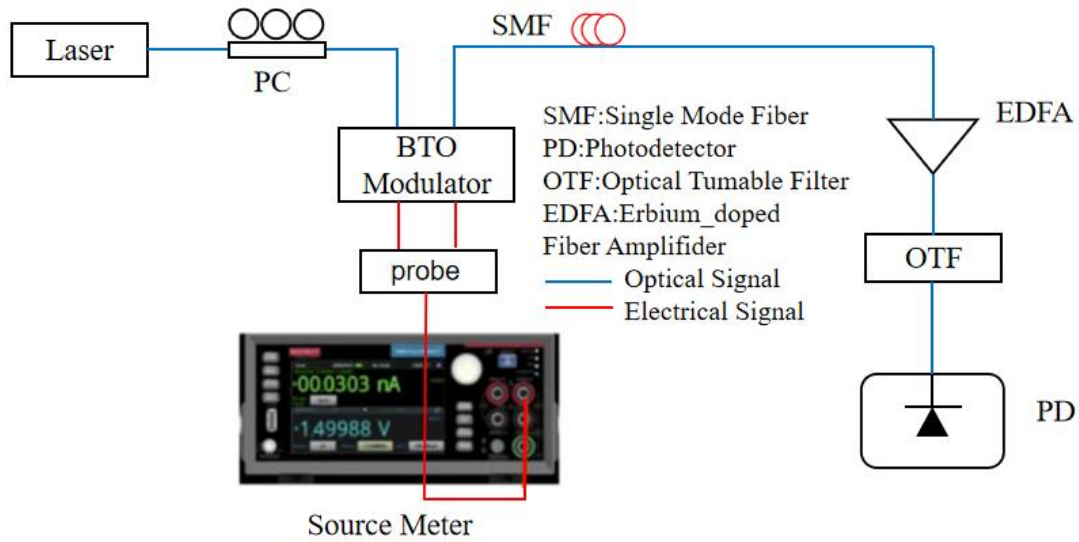


**Figure S7.** Schematic diagram of the experimental setup.

### Supporting Note 8: MZIs spectral responses

Figure S8 shows the transmission responses before and after transferring the ferroelectric films. Comparing with the curve before the transfer, it can be found that the output loss increased by  $\sim 1$  dB after transferring. We can find that before and after transferring the BTO layer, the refractive index of the structure changed, which in turn affected the interference of the two arms, resulting in a change in the extinction ratio of MZI. The extinction ratio of the device can reach more than 30 dB at a wavelength of 1545 nm, and the insertion loss of the whole device is about 18 dB.

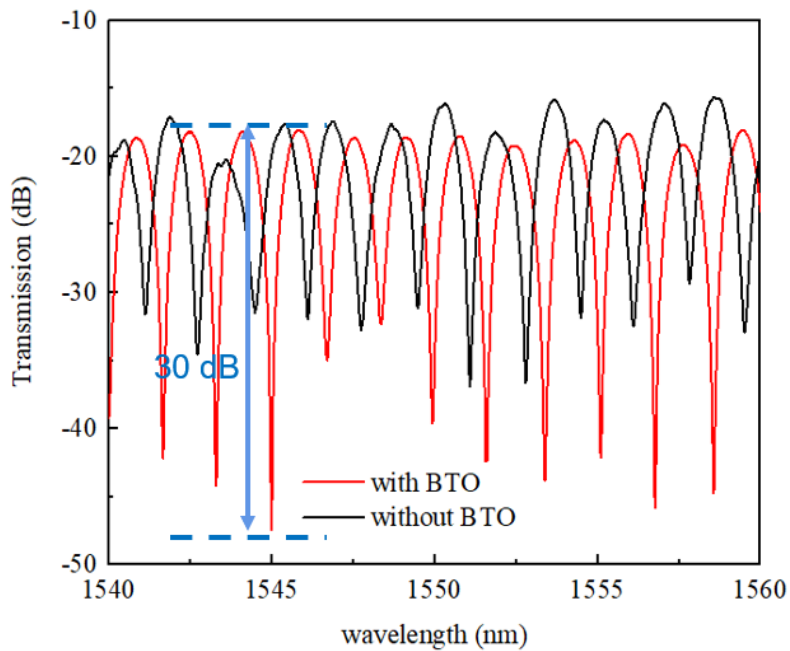


**Figure S8.** Transmission responses of the MZI before and after transferring the BTO layer.

### Supporting Note 9: Experimental curve of $\Delta n$ with different voltages

Using the relationship between  $\Delta\phi$  and  $\Delta n$  in Eq. 4, we can calculate the curve of  $\Delta n$  as a function of voltages as shown in Fig. S6. The red line in the graph is the tangent function of the curve, and the reciprocal of the slope of the tangent is proportional to the half-wave voltage. Comparing the simulation curves in Fig. 4, we can conclude that the experimental results correspond to the simulation results when the applied bias voltages changes from 0 to 10V.

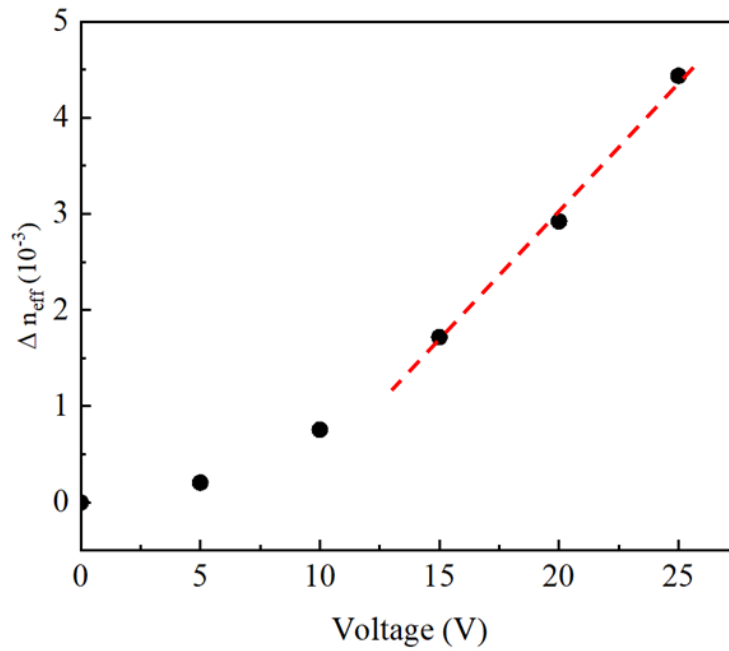


**Figure S9.** The change of the refractive index  $\Delta n$  with respect to different bias voltages.